Journal of Materials Chemistry A

Accepted Manuscript

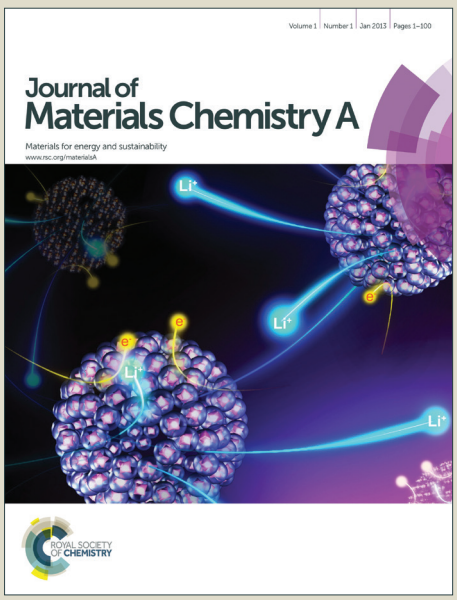

ROYAL SOCIETY OF CHEMISTRY

www.rsc.org/materialsA

Journal of Material Chemistry A

Cite this: DOI: 10.1039/c0xx00000x

www.rsc.org/ materials

PAPER

MnOOH/Nitrogen-Doped Graphene Hybrid Nanowires Sandwich Film for Flexible All-Solid-State Supercapacitors

Shuhua Yang, Xuefeng Song*, Peng Zhang and Lian Gao*

Received (in XXX, XXX) Xth XXXXXXXXX 20XX, Accepted Xth XXXXXXXXX 20XX

DOI: 10.1039/b000000x

All-solid-state supercapacitors (SCs) hold great promise as one of the most efficient energy storage devices due to its high power density, ease of use, and excellent reliability. However, its low energy density severely limits its practical application owing to the lack of suitable electrodes materials and reasonable electrode design. In this work, an advanced integrated electrode based on MnOOH/nitrogen-doped graphene hybrid nanowires sandwiched by annealing graphene oxide sheets (MNGHNs/AGO) with outstanding electrochemical performance was developed. The as-fabricated electrodes offer numerous pores for easy access of electrolyte, high conductivity for improved electron transport, high content (70 wt%) of MNGHNs for large electrochemical capacitance and energy density associated with the whole electrode, and effective protection and mechanical robustness for exceptional cycle life. With this intriguing architecture, MNGHNs/AGO all-solid-state SCs exhibit a volumetric capacitance as high as 26.3 F/cm^3 at 0.1 A/cm^3, a maximum energy density of up to 2.34 mWh/cm^3 at the power density of 0.04 W/cm^3, and an outstanding cycling stability of retaining 91.5% of the initial capacity even after 200,000 cycles at 5 A/cm^3. This work described here can provide a method for flexible, lightweight, low-cost, and high-performanced graphene-based sandwich films for supercapacitors.

1. Introduction

Supercapacitors (SCs), which store energy through either ion adsorption (electric double layer capacitance) or fast surface redox reactions (pseudocapacitance), are promising energy storage devices. Recently, great efforts have focused on flexible and thin all-solid-state SCs to cater for ever-increasing demands for flexible, wearable and rolling-up electronic devices.[1-3] For these applications, it is ideal to sophisticatedly select appropriate electrode materials and construct integrated electrode with designed configurations. It is well established that the electrochemical performances of these SCs are mainly determined by their composition, conductivity of the active materials, as well as the configuration of the integrated electrode, which are crucial for simultaneously achieving a high level of ion and electron transfer. Up to now, many nanostructured materials, such as metal oxides, conductive polymers, carbon materials, and their composites, etc, have been developed for use in SCs. Among them, manganese oxyhydroxide (MnOOH) is known to be a good candidate as SCs materials due to its low-cost, environmental benignity, and substantial specific capacitance.[4-6] Furthermore, metal oxyhydroxide has an inherent redox capability for facile electron-transfer processes and is the main electroactive species for the charge storage/delivery in the redox transition of the corresponding metal oxide.[5-9] However, the poor conductivity and chemical stability of MnOOH nanostructures drastically limit its application in SCs. Moreover, the reasonable design of advanced electrodes based on MnOOH nanostructures for SCs, simultaneously possessing good conductivity related to power density of the electrode and high mass loading associated with energy density of the electrode remains a great challenge.[10]

To improve the conductivity of active materials, an effective strategy is by combining with electrically conductive carbon materials. Among them, graphene, with the maximal surface area of 2630 m^2 g^{-1}, has received significant attention owing to its high conductivity, great chemical stability, and high mechanical flexibility.[11-13] However, only modest improvements in terms of the rate capability and capacitance have been obtained due to low conductivity and intrinsic capacitance of the as-synthesized graphene nanosheets.[14, 15] Recent achievements have demonstrated that chemical doping or surface functionalization with heteroatoms can effectively modify the electrical characteristics and chemical features of graphene, and thus remarkably improve the electrochemical performances of graphene.[16-18] Particularly, nitrogen-doped graphene (NG) has received increasing interest as electrode materials for SCs. It exhibits improved capacitance due to the modification of the electronic structure of the graphene by

* *State Key Laboratory for Metallic Matrix Composite Materials, School of Materials Science and Engineering, Shanghai Jiao Tong University, Shanghai, 200240, China. E-mail: liangao@mail.sic.ac.cn (L. Gao); songxfeng@sjtu.edu.cn (X. Song); Fax: +86-21-52413122; Tel: +86-21-52414301.*

† Electronic supplementary information (ESI) available. See DOI: 10.1039/ b000000x/

the N dopant.[16, 17, 19] Sun et al. have reported that nitrogen-doped graphene nanosheets represented much higher specific capacitance (326 F g^{-1}) than that of the reduced graphene oxide (203 F g^{-1}), and also exhibited a good cyclic stability and coulombic efficiency.[20] Analogous results have been also reported by Jeong and co-workers, which showed the specific capacitance was about 4 times larger than that of pristine graphene while keeping excellent rate capability.[19] Therefore, NG has great potential applications in SCs fields. Very recently, we reported a facile hydrothermal route to synthesize NG-based composite materials, which showed improved electrochemical properties.[21, 22] However, there are still some limitations on the electrochemical performance for those reported NG-based composite electrodes. For instance, most of active nanoparticles in such architectures only grow on the surface of graphene rather than being tightly wrapped between the graphene sheets, which results in the nanoparticles detachment from graphene sheets easily and severely degrades the electrochemical performance.[23]

Proper configuration of integrated electrode only consisting of pseudocapacitance materials and conducting support without any binding agents is a crucial and primary factor in achieving a better flexible all-solid-state SCs with high mass loading (energy density). Recent researches have demonstrated that the most promising electrode is the flexible freestanding film containing pseudocapacitance materials and conducting support prepared by the vacuum filtration method, in which all the components could participate in charge storage. Carbon nanotubes (CNTs) and reduced graphene oxide (RGO) nanosheets have attracted a lot of interest as conducting supports in flexible freestanding films using such method for SCs due to their extraordinary electrical properties, high chemical stability, and high mechanical stiffness, which have been applied as electrodes in flexible SCs with improved electrochemical performance. However, the electrode architectures using CNTs or RGO as conducting scaffold lead to a high fraction of dead volume in electrodes due to their inherent agglomerates or the additional surfactants or stabilizer for improving the water-soluble and film-forming ability, and thus result in drastic degradation in the overall energy density for SCs.[24, 25] In addition, most methods synthesizing such flexible freestanding films require complicated fabricating process (RGO) or the relatively high-cost raw materials (CNTs), which are expensive and difficult to upscale for their practical applications in SCs.[26, 27] To construct a desired flexible freestanding film with high loading mass based on conducting graphene support, a critical prerequisite is to fabricate a highly stable graphene with high oxygen content, exhibiting no any colloidal aggregation during electrode fabrication, especially when combining with other active nanomaterials. Recently, Kumar and coworkers presented a mild thermal annealing procedure to manipulate as-synthesized GO (also called "annealing graphene oxide" (AGO)) on a large scale, which can preserve the superiorly conductivity of graphene sheets while keeping a large number of oxygen content on graphene sheets.[28] The GO structures undergo a phase transformation into prominent oxidized and graphitic domains by temperature-driven oxygen diffusion. Consequently, such AGO structures are highly stable, and the conductivity simultaneously increases by up to four orders of magnitude, which should be a promising candidate as an ideally conducting support for flexible freestanding film electrodes in SCs applications.

Here, we developed a simple approach for *in situ* synthesizing single-crystalline MnOOH/nitrogen-doped graphene hybrid nanowires (MNGHNs) for the first time and subsequently the MNGHNs were sandwiched between AGO sheets by vacuum filtering method, forming the unique flexible freestanding sandwich film (MNGHNs/AGO). This sandwich architecture has the following characteristics: (1) the interconnected networks composed of the ultrathin MNGHNs 1D nanostructures provide a short diffusion length for electron and ion, in which numerously porous channels benefits the access of electrolyte and facilitates the rapid diffusion of electrolyte ions; (2) the nitrogen-doped graphene (NG) layer encapsulating MnOOH not only provides high conductivity, but also prevents the MnOOH from agglomeration and avoids the dissolution of MnOOH during the charge/discharge cycling; (3) the solution-processable AGO sheets concomitantly provide high conductivity and mechanical consolidation, which significantly improve the loading mass of active materials while keeping the good conductivity as an ideally conducting support. As a consequence, the as-prepared MNGHNs/AGO flexible freestanding electrodes with significant improvement in terms of capacitance, rate capability and cycling stability both in a three-electrode cell and symmetric all-solid-state SCs are envisaged. Such unique architectures not only provide high power density by facilitating rapid ion and electron transfers, but also possess high energy density by enhancing the loading mass of active materials (Table S1 in the ESI†).

2. Experimental

2.1 Synthesis of MNGHNs

Graphene oxide (GO) was prepared from natural flake graphite (Alfa Aesar, 325 mesh, 99.8%) using a modified Hummers method, as described elsewhere.[29] For the preparation of MnOOH/nitrogen-doped graphene hybrid nanowires (MNGHNs), 158 mg $KMnO_4$ was dispersed in 30 ml Milli-Q water. Then the solution was added into 50 ml of 1 mg/mL GO suspension and stirred for 15 min at room temperature. Afterwards, 3 mL of formamide was added to the above suspension. The obtained mixture solution was transferred to a Teflon-lined autoclave for hydrothermal reaction at 110 °C for 6 h. The final product (MNGHNs) was collected by centrifuge and washed with Milli-Q water and absolute ethanol, and then dried at 60 °C in a vacuum oven overnight. For comparison, graphene oxide-MnOOH nanowire composites (GMWs) and MnOOH nanowires were prepared according to previous reports.[6, 30]

2.2 Preparation of AGO

The annealing GO (AGO) was prepared by a mild thermal annealing procedure according to the method presented by Priyank V. Kumar and colleagues.[28] Briefly, the GO obtained was suspended in 320 ml of water to get a 0.5 mg/mL GO suspension. The GO suspension was put in a sealed glass bottle and kept in a vacuum oven at 80 °C for 10 days. Then the as-prepared suspension was stored at room temperature. It was observed that the annealing GO suspension was still stable after several months.

2.3 Fabrication of flexible freestanding MNGHNs/AGO sandwich film

The flexible freestanding MNGHNs/AGO sandwich film was fabricated simply by the vacuum filtration method. MNGHNs were dispersed in Milli-Q water (100 mL) followed by ultrasonication for 15 min. Then the AGO suspension was mixed with the as-prepared MNGHNs solution and sonicated for another 15 min to ensure the sufficient mixing of them (The MNGHNs in MNGHNs/AGO sandwich film was about 70%). Finally, the as-obtained solution was filtered through a mixed cellulose ester filter membrane (0.22 μm pore size), followed by drying in the air, peeling from the membrane, and then getting the freestanding MNGHNs/AGO sandwich film. For comparison, reduced graphene oxide (RGO) was prepared by the method reported by Dan Li etc.[31] A similar process to MNGHNs/AGO sandwich film was then applied in the preparation of MNGHNs/RGO, GMWs/AGO, and MnOOH/AGO sandwich films.

2.4 Assembling of the flexible all-solid-state SCs

The all-solid-state SCs were assembled in a symmetrical configuration using a similar procedure reported by Xiao et al.[32] Two pieces of MNGHNs/AGO sandwich films (10 mm×20 mm) were glued with a nickel slice by conducting silver paste, and then were sandwiched by PVA/H_3PO_4 gel as solid-state electrolyte with a separator (NKK TF40, 30 μm). After assembling, the PVA/H_3PO_4 gel was solidified at room temperature to obtain the all-solid-state SC. PVA/H_3PO_4 gel electrolyte was simply prepared as follows: 6 g of H_3PO_4 was added into 60 mL of Milli-Q water under vigorous stirring. 6 g of PVA power was then added into the above solution. The final mixture was heated to 85°C under stirring until all the chemicals were fully dissolved and the solution became clear.

2.5 Material Characterization

The X-ray diffraction (XRD) patterns were measured on a Goniometer Ultima IV (185 mm) diffractometer with Cu Kα radiation (λ= 1.5418 Å) at a step of 0.02° per second. Field emission scanning electron microscopy (FESEM) and scanning transmission electron microscopy (STEM) were carried out on a JSM-6700F scanning electron microscope. Transmission electron microscopy (TEM) was carried out on a JEOL JEM-2010F 200 kV transmission electron microscope. Raman spectra were conducted using a DXR Raman Microscope with an excitation length of 532 nm. X-ray photoelectron spectroscopy (XPS) was performed on a Kratos AXIS Ultra DLD spectrometer. Thermogravimetric analyses (TGA) were run on a SDT Q600 V20.9 Build 20 thermogravimetric analyzer at a heating rate of 10 °C min^{-1} from 30 to 850 °C in air. Nitrogen sorption isotherms and the Brunauer-Emmett-Teller (BET) surface area of the as-prepared samples were investigated by an Autosorb-iQ-C-TCD.TRX full-automatic physical and chemical adsorption analyzer at 77 K.

2.6 Electrochemical Measurements.

All the electrochemical measurements were carried out using a VMP3 multi-functional electrochemical analysis instrument (Bio-Logic, France). The capacitive performance of the individual electrode was performed in a three-electrode cell in 1 M Na_2SO_4 aqueous solution. The flexible freestanding MNGHNs/AGO sandwich film (about 1 cm×1 cm) was directly used as electrode and current collector, while a platinum foil (1 cm×1 cm) and an Ag/AgCl electrode were used as the counter and reference electrode, respectively. The working electrode was soaked in 1 M Na_2SO_4 solution for 2 h before the electrochemical test to improve wettability of the electrode. Electrochemical behaviour of both individual electrode and all-solid-state SCs were investigated by the means of cyclic voltammetry and galvanostatic charge/discharge measurements. The cyclic voltammograms were recorded within a potential window of 0 to 0.8 V at different scanning rates. The galvanostatic charge/discharge measurements were performed at different current densities.

3. Results and discussion

The microstructure and morphology of the MNGHNs was characterized by scanning electron microscopy (SEM) and transmission electron microscopy (TEM). It can be seen from the representative SEM (Fig. S1 in the ESI†) and TEM (Fig. 1a) images that the entangled nanowires have a high aspect ratio with lengths up to hundreds of nanometers and diameters down to ca. 10 nm. Remarkably, as shown in the zoom-in TEM image (Fig. 1b), MnOOH nanowires were tightly wrapped by graphene sheets as indicated by the red arrows, which benefit to preventing MnOOH nanowires from agglomeration and avoiding the dissolution of MnOOH during the charge/discharge cycling.[27] A high-resolution TEM (HRTEM) image clearly shows the interface between graphene and MnOOH (Fig. 1c). The lattice fringes of graphene can be obviously identified due to the distortions of graphene structure caused by the intercalation of nitrogen atoms (as indicated by the arrow in Fig. 1c).[33] Meanwhile, the HRTEM images and the FFT pattern indicate that the formed nanowires are

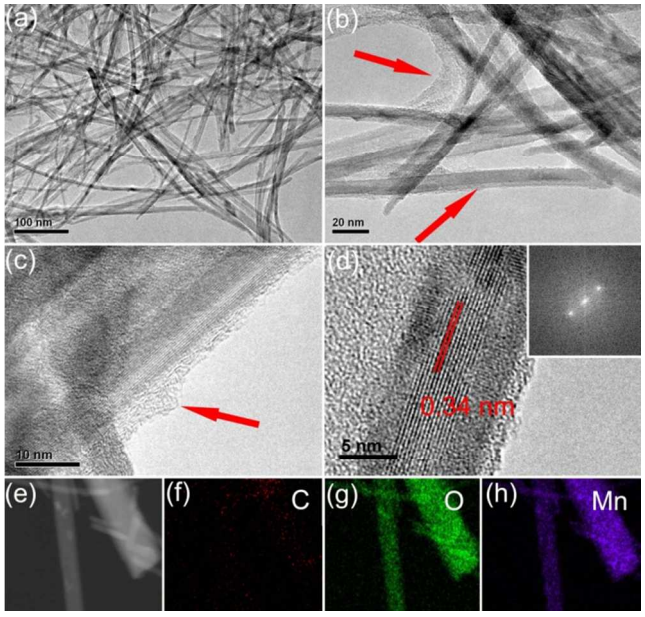

Fig. 1 (a) TEM image, (b) Zoom-in TEM image, and (c, d) HRTEM images of MNGHNs; inset in (d) shows FFT pattern of MnOOH. (e) Scanning transmission electron microscopy (STEM) image of MNGHNs and corresponding elemental mapping of (f) carbon, (g) oxygen, and (h) manganese.

single crystalline (Fig. 1c, d). Lattice fringes can be discerned in Fig. 1d with a distinct lattice spacing of 0.34 nm, which corresponds to the $(11\bar{1})$ planes of MnOOH. The structure and

composition of the MNGHNs is further analyzed by energy-dispersive X-ray spectroscopy elemental mapping. As presented in Fig. 1e-h, carbon, oxygen, and manganese atoms are homogeneously distributed in all of the MnOOH nanowires, highlighting the uniform coating of graphene sheets on MnOOH nanowires.

Fig. 2a shows the X-ray diffraction (XRD) pattern of the MNGHNs, indicating the formation of MnOOH (JCPDS no. 41-1379). Importantly, no obvious peak at ~25º is detected, which suggest that highly disordered and few-layer graphene sheets are uniformly dispersed in the MNGHNs, consistent with the aforementioned TEM images. More information about the structure of the MNGHNs, MnOOH and NG can be obtained from Raman spectroscopy. As shown in Fig. 2b, there are two prominent peaks at 1349 and 1575.5 cm^{-1} for NG, which correspond to the D and G bands of NG, respectively.[34] However, the G band of the MNGHNs remarkably shifts from 1575.5 cm^{-1} to 1586 cm^{-1} compared with NG, revealing the electronic interactions between NG and MnOOH nanowires, which will benefit electron transportation between NG and MnOOH nanowires and thus improve the rate capability.[21, 35] The other three peaks located at 352, 383, and 553 cm^{-1} were observed in both MNGHNs and pure MnOOH, attributed to the MnOOH phase. From the relative intensities of the D and G band peaks, it can be concluded that a higher concentration of structure defects exist in MNGHNs (I_D/I_G= 1.16) relative to the NG (I_D/I_G= 1.04). It has been demonstrated that the defects of graphene can store more electrons due to

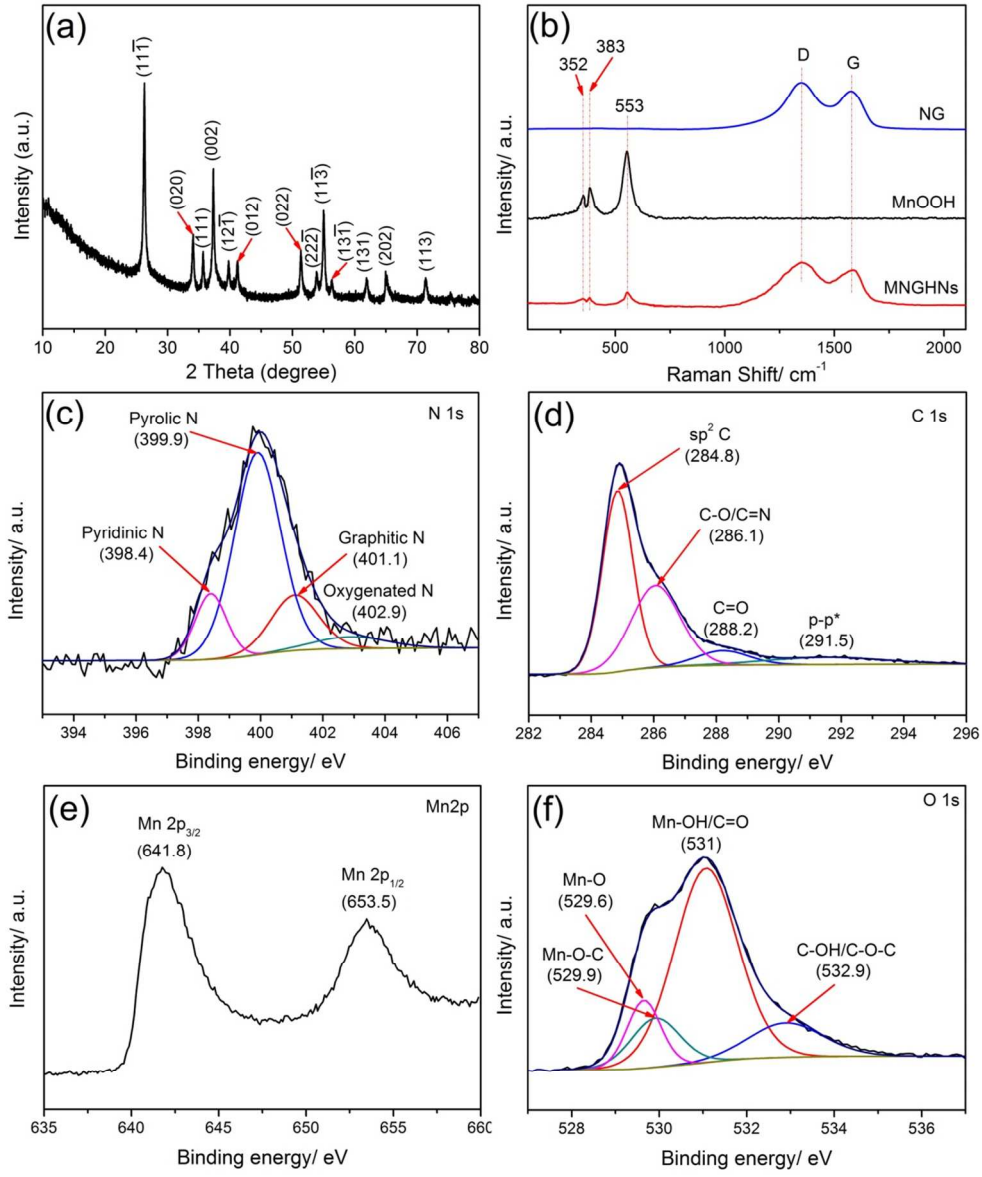

Fig. 2 (a) XRD pattern of MNGHNs, (b) Raman spectra of MNGHNs, MnOOH, and NG, (c) N 1s narrow spectra of MNGHNs, (d) C 1s narrow spectra of MNGHNs, (e) Mn 2p narrow spectra of MNGHNs, (f) O 1s narrow spectra of MNGHNs.

abundant active sites resulting from the defects, considerably enhancing the specific capacitance of the composites.[19, 22] The weight percentage of MnOOH in the composite is 75.2 wt %, determined by thermogravimetric analysis (TGA) as shown in Fig. S2 in the ESI†.

The chemical binding state of the as-prepared MNGHNs was obtained by X-ray photoelectron spectroscopy (XPS) measurements. The survey spectrum clearly discloses the existence of N in the MNGHNs, which is estimated to be 4.92 atom% (Fig. S3 in the ESI†). A Gaussian fit to the N 1s spectrum of the MNGHNs shows four N-containing groups are possibly present, which correspond to pyridinic N (398.4 eV), pyrolic N (399.9 eV), graphitic N (401.1 eV), and oxygenated N (402.9 eV), respectively (Fig. 2c). Based on the area ratio of the XPS peaks, the contents of pyridinic N, pyrolic N, graphitic N, and oxygenated N are 13.8%, 62.6%, 17.8%, and 5.8%, respectively, among which the dominant pyrolic N and the pyridinic N play a crucial role in improving the electrochemical properties of graphene due to better electron-donor characteristics, while the graphitic N can increase the conductivity of graphene in the electrochemical process.[19, 22] The high resolution C 1s peak can be decomposed into four apparent peaks, which could be ascribed to sp^2 C (284.8 eV), C-O/C=N (286.1eV), C=O (288.2 eV), and p-p* (291.5 eV) (Fig. 2d).[36, 37] In the spectra of Mn 2p, the peaks located at 641.8 and 653.5 are attributed to the Mn $2p_{3/2}$, and Mn $2p_{1/2}$ for the MnOOH nanowires, which are in good agreement with previous report on MnOOH (Fig. 2e)[38]. From the high resolution O1s spectrum shown in Fig. 2f, the spectrum could be fitted with four peaks at 529.6, 529.9, 531 and 532.9 eV, corresponding to Mn-O, Mn-O-C, Mn-OH/C=O, and C-OH/C-O-C, respectively.[22, 38] Additionally, compared with the peak at 532.7 eV in the O 1s XPS spectrum of the graphene (Fig. S4 in the ESI†), the contents of the C-O-C group in the MNGHNs (Fig. 2f) are obviously decreased, demonstrating a possible ring-opening reaction of epoxy groups by the manganese ion in MnOOH, forming the Mn-O-C bond.[29, 39] It is also noted that the MnOOH does not separate from graphene sheets even under long-time ultrasonication treatment, confirming the strong attachment between the MnOOH and the NG sheets.

The flexible freestanding MNGHNs/AGO sandwich film was obtained by vacuum filtration of the mixed aqueous solution of the MNGHNs and AGO through a mixed cellulose ester filter membrane (0.22 μm pore size), followed by drying in air, and then peeling from the membrane, similar to the method reported for making GO paper.[31] The fabrication procedures and architectural features of MNGHNs/AGO sandwich film were illustrated in Fig. 3a. The digital images (Fig. 3b) show that the flexible freestanding MNGHNs/AGO sandwich film exhibits metallic luster and high flexibility. Furthermore, the sandwich film also exhibits good film-forming ability compared with the MNGHNs/RGO sandwich film when the percentage of MNGHNs content in the film increases (Fig. S5 in the ESI†). The cross-section SEM image of the flexible freestanding MNGHNs/AGO sandwich film (Fig. 3c) shows that well-distributed MNGHNs are homogeneously sandwiched between AGO sheets, forming a three-dimensionally

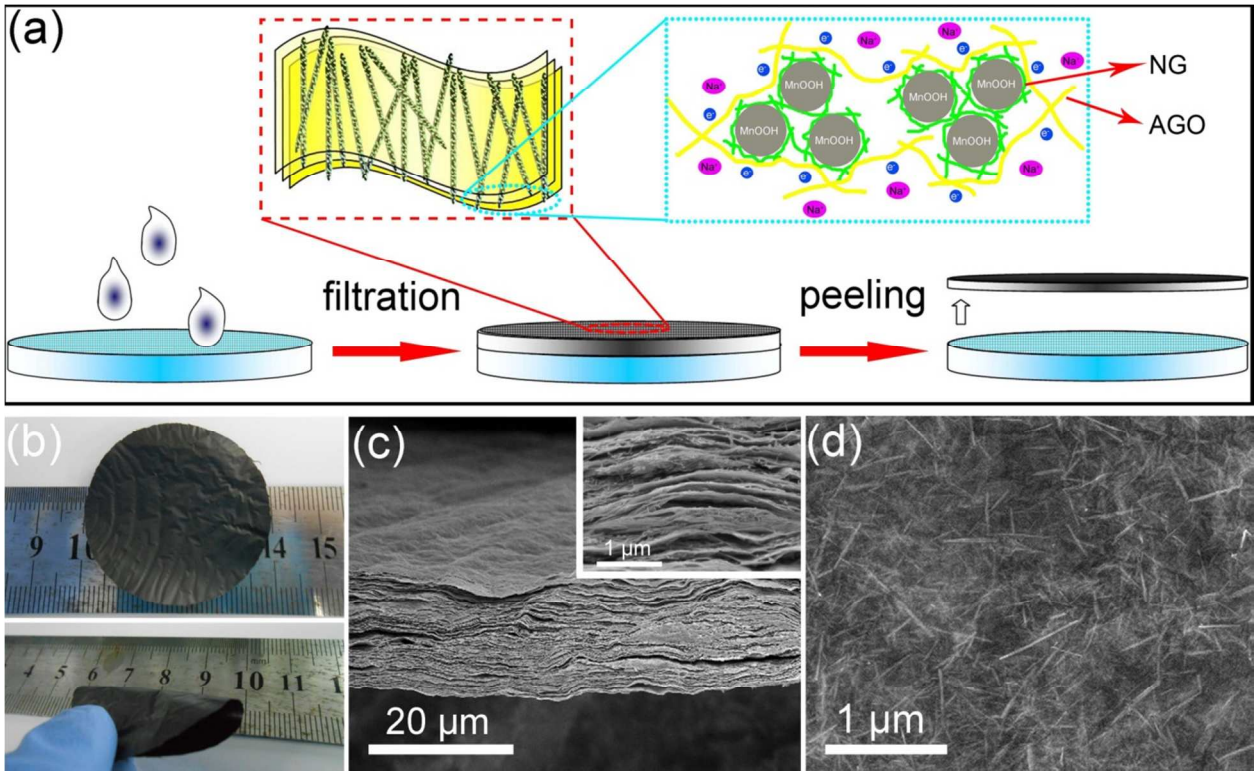

Fig. 3 (a) Schematic fabrication procedures and architectural features of MNGHNs/AGO sandwich film, (b) Digital images of flexible freestanding MNGHNs/AGO sandwich film, (c) Cross-section SEM image of the flexible freestanding MNGHNs/AGO sandwich film, (d) Top-surface SEM image of the flexible freestanding MNGHNs/AGO sandwich film. The inset in (c) is the enlarged cross-section image of the flexible freestanding MNGHNs/AGO sandwich film.

layered and wrinkled structure. The top-surface SEM image (Fig. 3d) further manifests the MNGHNs and AGO are well linked together and MNGHNs are distributed uniformly in the AGO matrix to form a MNGHNs/AGO sandwich film. Such unique architectures (as shown in Fig. 3a) can provide (1) numerously porous channels for the access of electrolyte owing to the interconnected networks of ultrathin MNGHNs nanowires (ca. 10 nm), facilitating rapid diffusions of ions within the film electrode and enabling better utilizations of the pseudocapacitance of MNGHNs, (2) abundant active sites resulting from the defects of nitrogen doping, which lead to adsorption of more ions and rapid electron transfers, (3) an extraordinary conductivity of the overall electrode derived from the interconnected MNGHNs and AGO networks, and (4) the high content of MNGHNs within the film electrode (up to 70% by weight), thereby improving MnOOH utilizations, which can effectively improve the electrochemical capacitance and energy density of the whole electrode. The synergy of the MNGHNs and AGO with the sufficient utilizations of active materials is regarded to substantially reduce the diffusion paths of ions, significantly accommodate more electroactive species, and provide an excellent conductivity and high flexibility, which are beneficial to obtain high electrochemical performance associated with the flexible freestanding MNGHNs/AGO sandwich film.

The electrochemical properties of the flexible freestanding MNGHNs/AGO sandwich film were examined in a three-electrode cell using 1 M Na_2SO_4 aqueous solution as the electrolyte, a platinum foil (1 cm ×1 cm) as the counter electrode, and a Ag/AgCl electrode as the reference electrode. Fig. 4a shows the cyclic voltammograms (CV) of the flexible freestanding MNGHNs/AGO sandwich film in a potential window between 0 and 0.8 V at different scan rates. It can be evidently observed that the CV curves essentially present the same shape as the scan rate increases from 5 to 100 mV/s and display nearly mirror images, indicating the good capacitive behavior of the MNGHNs/AGO sandwich film. The charge/discharge (CD) curves of the flexible freestanding MNGHNs/AGO sandwich films at different current densities are given in Fig. 4b. It can be seen that the charging curves and their corresponding discharging counterparts are all nearly symmetrical and there is no obvious potential drop (IR drop), revealing the exceptional capacitive reversibility during the electrochemical processes. The low internal resistance of the MNGHNs/AGO sandwich film was further demonstrated by electrochemical impedance spectroscopy (EIS) measurements (Fig. S6a in the ESI†). Equivalent series resistance (ESR) estimated from the intersection point on the real axis was as small as 1.2 Ω. The Nyquist plot was well-fit to a complex equivalent circuit as shown in Fig. S6b in the ESI†. The areal capacitance for the MNGHNs/AGO sandwich film is calculated from the discharge curves (for details, see the ESI†). The MNGHNs/AGO sandwich film achieves an excellent areal capacitance of 173.2 mF/cm^2 at current densities of 1mA/cm^2, which is much higher than that of conventional carbon-based electrodes[40, 41] and comparable to other manganese oxide-based electrodes reported previously (Table S2

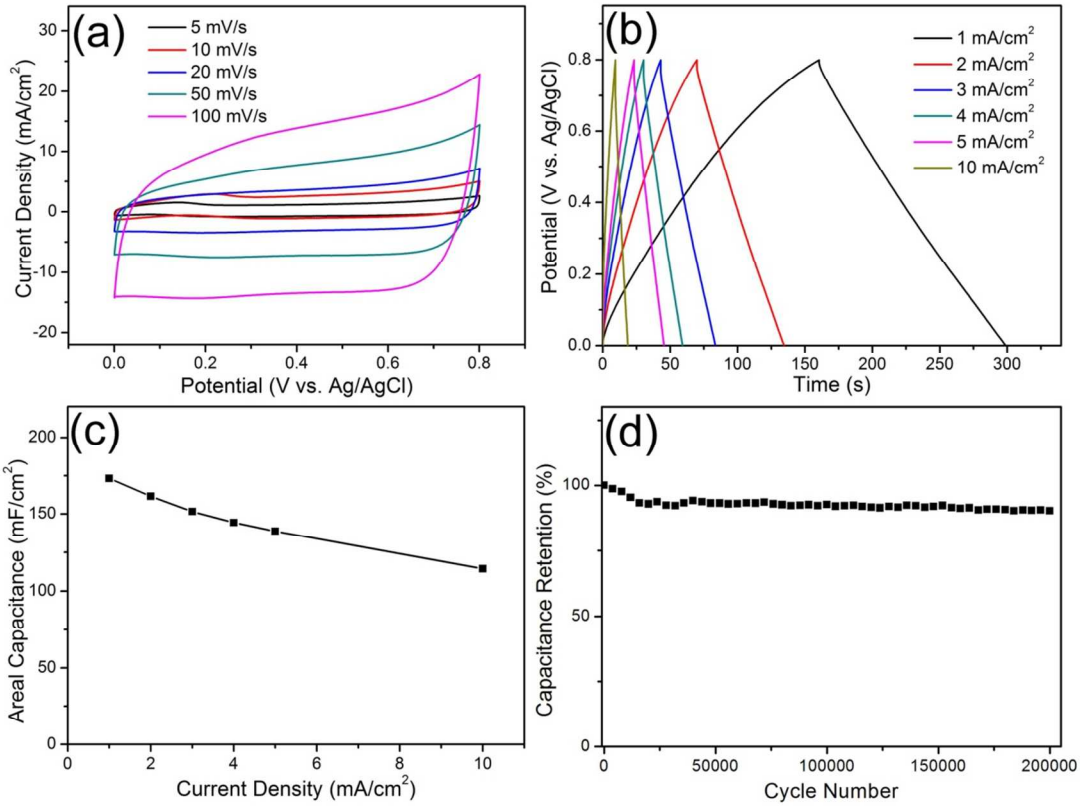

Fig. 4 (a) CV curves and (b) CD curves of the flexible freestanding MNGHNs/AGO sandwich film by a three-electrode configuration in 1 M Na_2SO_4 aqueous solution. (c) Areal capacitance of the flexible freestanding MNGHNs/AGO sandwich film at various current densities. (d) Cycle life of the flexible freestanding MNGHNs/AGO sandwich film at 50 mA/cm^2.

in the ESI†). It should be noted that there is still around 66.1% initial capacitance retention even when the current density increases from 1 to 10 mA/cm^2, indicating an excellent rate capability (Fig. 4c). For comparison, the CV and CD curves of the MNGHNs/RGO, GMWs/AGO, and MnOOH/AGO sandwich films are also carried out under the same test conditions, as shown in Fig. S7 in the ESI†. It is evident that their electrochemical performances are far less satisfactory than that of the MNGHNs/AGO sandwich film. Moreover, even at a high current density of 50 mA/cm^2, the areal capacitance of the MNGHNs/AGO sandwich film still retains 90.2% of its initially areal capacitance after 200,000 cycles (Fig. 4d). A similar phenomenon of continuous decrease associated with the capacitance in aqueous solution with the increase of cycle number is also found in other literatures, attributing to the irreversible oxidation reaction and phase change of metal oxides or hydroxides.[10, 42-45] It should be noted that the cyclic stability of the MNGHNs/AGO sandwich film is among the highest ever reported for manganese oxide-based electrodes (Table S2 in the ESI†), which can be ascribed to the simultaneous dissolution/transformation between various manganese oxide and the ultrathin NG coating, an effective barrier to the electrolyte, protecting the MnOOH nanowires from electrochemical dissolution. The superior electrochemical performance of MNGHNs/AGO sandwich film can be attributed to the large accessible surface area of the MNGHNs (177.6 m^2 g^{-1} as shown in Fig. S8 in the ESI†), as well as the enhanced conductivity of the sandwich film due to the wrapped NG on the MnOOH surface and the direct contact between AGO and MNGHNs without any other binders. Moreover, the dual encapsulation of NG and AGO favorably enables MnOOH stable, and prevents the direct contact of MnOOH nanowires with the electrolyte, securing the integrity of MnOOH nanowires during charge/discharge cycling.

To evaluate that the as-synthesized flexible freestanding MNGHNs/AGO sandwich film can be applied to flexible electronics or devices, we prepared flexibly symmetric all-solid-state SCs, in which the flexible freestanding MNGHNs/AGO sandwich film was directly used as both working electrode and current collector without any binding agents or conducting additives, and H_3PO_4/PVA gel was served as the solid-state electrolyte. The as-fabricated SC is highly flexible and mechanically stable, and can be bended (Fig. 5a) without destroying the structural integrity of the device. Fig. 5b shows the CV curves of the MNGHNs/AGO all-solid-state SCs at different bending angles with a potential window from 0 to 0.8 V. According to the CV curves, almost no change of the electrochemical response was observed under different bending

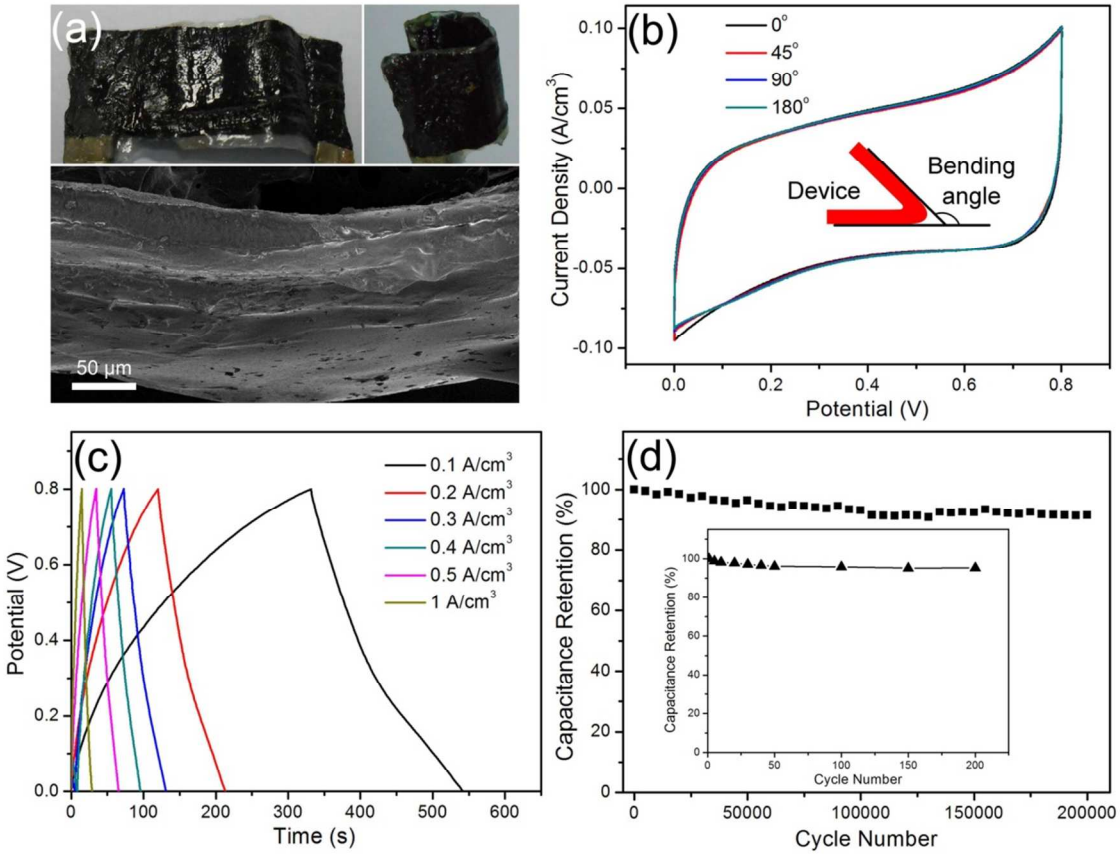

Fig. 5 (a) Optical photographs and cross-sectional SEM image of the fabricated all-solid-state SCs, (b) CV curves for MNGHNs/AGO all-solid-state SC under different curvatures of 0º, 45º, 90º, and 180º at a scan rate of 10 mV/s. (c) CD curves for MNGHNs/AGO all-solid-state SC under a curvature of 90º at different current densities. (d) Cycling stability of MNGHNs/AGO all-solid-state SC at a current density of 5 A/cm^3. Inset shows cycling performance of the flexible supercapacitors for 200 bending cycles at a current density of 5 A/cm^3.

condition, demonstrating that the MNGHNs/AGO all-solid-state SCs have an excellent flexibility and mechanical stability. In addition, the rectangular profile and symmetry of CVs show the ideal capacitive behavior of MNGHNs/AGO and low contact resistance.[46] The CD curves at various current densities exhibit a symmetric linear profile (Fig. 5c), revealing the good capacitive reversibility of the all-solid-state SCs. The volumetric capacitance of the all-solid-state SCs device (including electrodes, separator and electrolyte) was measured to be 26.3 F/cm^3 at 0.1 A/cm^3. More strikingly, it still delivers a high capacitance of around 17.3 F/cm^3 even at 1 A/cm^3, indicating the fast charge/discharge feature and excellent retention capability (Fig. 5c), which is probably attributed to the proper incorporation of electrolyte into the layered structure with numerously porous channels, fast ion diffusions in all-solid-state device and an high conductivity of the sandwich film.[47, 48] Such an excellent volumetric capacitance based on the whole SCs is considerably higher than that of previously reported electrode materials used for flexibly all-solid-state SCs, such as graphene (0.45 F/cm^3),[1] carbon/MnO_2 (2.5 F/cm^3),[49] and VN/CNT (7.9 F/cm^3).[32] The electrochemical impedance spectroscopy (EIS) measurements also confirmed the lower internal resistance and faster electrolyte diffusion (Fig. S9 in the ESI†).[46] The volumetric energy and power density of the entire device have been widely used to evaluate the performance of all-solid-state SCs. The Ragone plots depict the energy-power characteristics of the as-fabricated MNGHNs/AGO films for all-solid-state SCs, comparing with the performance of different energy storage devices reported (Fig. S10 in the ESI†). The maximum energy density up to 2.34 mWh/cm^3 is achieved at the power density of 0.04 W/cm^3, and remains 1.54 mWh/cm^3 at 0.4 W/cm^3, which are larger than a similar system based on VN/CNT all-solid-state SCs (0.54 mWh/cm^3)[32] and most of carbon/graphene based all-solid-state SCs (Table S3 in the ESI†), and even superior to hydrated graphite oxide (0.43 mWh/cm^3)[40] and onion-like carbon SCs in liquid electrolyte (1.5 mWh/cm^3).[41]

For practical application, the cycling performance and the leakage current and self-discharge characteristics were also measured to evaluate the electrochemical performance of MNGHNs/AGO all-solid-state SCs. Fig. 5d shows the volumetric capacitance still remains 91.5% of the initial capacitance even after 200,000 charge/discharge cycles at a high current density of 5 A/cm^3, demonstrating excellent electrochemical stability and a high level of reversibility of as-fabricated flexible device. The flexibility lifetime of the flexible supercapacitor was also tested, as shown in the inset in Fig. 5d. Even after 200 bending actions, the resulting specific capacitance retained 95.3% of its initial value, further confirming its excellent mechanical and flexible properties. As shown in Fig. S11a in the ESI†, the leakage current through the device quickly stabilizes at 0.0112 mA and is stable at such value for a long time beyond 2 h, indicating a relatively high stability of the fabricated device.[46, 50] The stability of the device was further confirmed by a self-discharge test represented by the time course of the open-circuit voltage (Fig. S11b in the ESI†). The MNGHNs/AGO all-solid-state SC device underwent a rapid self-discharge process in the first few minutes and gradually slowed for several hours. Finally, the open-circuit voltage of the device maintained at about 0.3 V beyond 30 h, which is higher than or comparable to previous results of all-solid-state SCs.[46, 48, 50]

These results demonstrate that as-fabricated devices exhibit excellent cycling stability, low leakage current, and low self-discharge characteristics, which are highly desirable for practical applications.

To further estimate the practical usage of the flexible all-solid-state SCs based on the flexible freestanding MNGHNs/AGO electrodes, we connected three identical SC units in series or parallel to construct an assembled device and control over the operating voltage and energy storage. The galvanostatic CD measurements of the individual device, and three devices connected in series and parallel were performed at the same conditions, which can be seen in Fig. S12 in the ESI†. The tandem devices exhibit a very good control over the potential window (about 2.4 V) with almost the same discharge time compared with a single device, and deliver essentially ideal triangular charge/discharge curves, indicating excellent capacitive performance of each all-solid-state SC (Fig. S12a in the ESI†). Moreover, the discharge time of parallel devices was about 3 times longer than an individual device (Fig. S12b in the ESI†), which is in accordance with the theoretical time, indicating nearly ideal capacitive characteristics of the fabricated MNGHNs/AGO all-solid-state SC.

4. Conclusions

In summary, MnOOH/nitrogen-doped graphene hybrid nanowires (MNGHNs) are successfully prepared by a facile one-step strategy for the first time. Subsequently, a novel kind of self-standing binder-free sandwich film (MNGHNs/AGO) has been successfully synthesized via the encapsulation of MNGHNs with AGO mantles. In such intriguing architecture, the MnOOH nanowires are wrapped by NG sheets and sandwiched with AGO mantles, which provides a better conductive network and appropriate porous channels, effectively establishing a rapid electron transfer path as well as allowing easy diffusions of electrolyte into the inner region of the electrode. In addition, the dual encapsulation (NG and AGO nanosheets) effectively inhibits the dissolution and fusion of MnOOH nanowires during the charge/discharge process, and obviously increases the loading mass in the whole electrode, thus delivering exceptionally structural stability and high energy density of the electrode. The all-solid-state SCs based on flexible freestanding MNGHNs/AGO electrodes exhibit a maximum energy density of up to 2.34 mWh/cm^3 at the power density of 0.04 W/cm^3, while keeping exceptional cycling stability and better rate capacity. While the all-solid-state SC based on flexible freestanding MNGHNs/AGO electrodes holds significant features such as high flexibility, easy assembly in series and parallel, and excellent electrochemical performance, the electrode design throws light on a new avenue for developing high-performance electrode materials for the flexible or wearable devices application.

Acknowledgements

The authors greatly acknowledge the financial support by the National Natural Science Foundation of China (51302169, 51172142), the Shanghai Municipal Natural Science Foundation (12ZR1414300), the SJTU-SMC Foundation for Excellent Young Teacher, and the Third Phase of 211 Project for Advanced

Materials Science (WS3116205007).

Notes and references

1. M. F. El-Kady, V. Strong, S. Dubin and R. B. Kaner, *Science*, 2012, **335**, 1326-1330.
2. X. Lu, M. Yu, G. Wang, T. Zhai, S. Xie, Y. Ling, Y. Tong and Y. Li, *Adv. Mater.*, 2013, **25**, 267-272.
3. F. Liu, S. Song, D. Xue and H. Zhang, *Adv. Mater.*, 2012, **24**, 1089-1094.
4. Z. Li, H. Bao, X. Miao and X. Chen, *J. Colloid Interface Sci.*, 2011, **357**, 286-291.
5. H. T. Tan, X. Rui, W. Shi, C. Xu, H. Yu, H. E. Hoster and Q. Yan, *ChemPlusChem*, 2013, **78**, 554-560.
6. L. Wang and D. L. Wang, *Electrochim. Acta*, 2011, **56**, 5010-5015.
7. H. Li, M. Yu, F. Wang, P. Liu, Y. Liang, J. Xiao, C. Wang, Y. Tong and G. Yang, *Nat. Commun.*, 2013, **4**, 1894.
8. H. Li, M. Yu, X. Lu, P. Liu, Y. Liang, J. Xiao, Y. Tong and G. Yang, *ACS Appl. Mater. Interfaces*, 2014, **6**, 745-749.
9. M. Toupin, T. Brousse and D. Bélanger, *Chem. Mater.*, 2004, **16**, 3184-3190.
10. J. Jiang, Y. Li, J. Liu, X. Huang, C. Yuan and X. W. D. Lou, *Adv. Mater.*, 2012, **24**, 5166-5180.
11. X. Huang, Z. Zeng, Z. Fan, J. Liu and H. Zhang, *Adv. Mater.*, 2012, **24**, 5979-6004.
12. S. Yang, X. Song, P. Zhang, J. Sun and L. Gao, *Small*, 2014, **10**, 2270-2279.
13. C. Xu, B. Xu, Y. Gu, Z. Xiong, J. Sun and X. Zhao, *Energy Environ. Sci.*, 2013, **6**, 1388-1414.
14. Z. Fan, J. Yan, T. Wei, L. Zhi, G. Ning, T. Li and F. Wei, *Adv. Funct. Mater.*, 2011, **21**, 2366-2375.
15. S. W. Lee, J. Kim, S. Chen, P. T. Hammond and Y. Shao-Horn, *ACS Nano*, 2010, **4**, 3889-3896.
16. E. Paek, A. J. Pak, K. E. Kweon and G. S. Hwang, *J. Phys. Chem. C*, 2013, **117**, 5610-5616.
17. L. L. Zhang, X. Zhao, H. Ji, M. D. Stoller, L. Lai, S. Murali, S. Mcdonnell, B. Cleveger, R. M. Wallace and R. S. Ruoff, *Energy Environ. Sci.*, 2012, **5**, 9618-9625.
18. Z. Wen, X. Wang, S. Mao, Z. Bo, H. Kim, S. Cui, G. Lu, X. Feng and J. Chen, *Adv. Mater.*, 2012, **24**, 5610-5616.
19. H. M. Jeong, J. W. Lee, W. H. Shin, Y. J. Choi, H. J. Shin, J. K. Kang and J. W. Choi, *Nano Lett.*, 2011, **11**, 2472-2477.
20. L. Sun, L. Wang, C. Tian, T. Tan, Y. Xie, K. Shi, M. Li and H. Fu, *RSC Adv.*, 2012, **2**, 4498-4506.
21. C. Xu, J. Sun and L. Gao, *Nanoscale*, 2012, **4**, 5425-5430.
22. S. Yang, X. Song, P. Zhang and L. Gao, *ACS Appl. Mater. Interfaces*, 2013, **5**, 3317-3322.
23. X. Wang, X. Cao, L. Bourgeois, H. Guan, S. Chen, Y. Zhong, D. M. Tang, H. Li, T. Zhai and L. Li, *Adv. Funct. Mater.*, 2012, **22**, 2682-2690.
24. L. Hu, W. Chen, X. Xie, N. Liu, Y. Yang, H. Wu, Y. Yao, M. Pasta, H. N. Alshareef and Y. Cui, *ACS Nano*, 2011, **5**, 8904-8913.
25. Z. Weng, Y. Su, D. W. Wang, F. Li, J. Du and H. M. Cheng, *Adv. Energy Mater.*, 2011, **1**, 917-922.
26. D. Eder, *Chem. Rev*, 2010, **110**, 1348-1385.
27. Y. He, W. Chen, X. Li, Z. Zhang, J. Fu, C. Zhao and E. Xie, *ACS Nano*, 2012, **7**, 174-182.
28. P. V. Kumar, N. M. Bardhan, S. Tongay, J. Wu, A. M. Belcher and J. C. Grossman, *Nat. Chem.*, 2014, **6**, 151-158.
29. S. Yang, X. Song, P. Zhang and L. Gao, *J. Mater. Chem. A*, 2013, **1**, 14162-14169.
30. Y. C. Zhang, T. Qiao and X. Ya Hu, *J. Solid State Chem.*, 2004, **177**, 4093-4097.
31. D. Li, M. B. Müller, S. Gilje, R. B. Kaner and G. G. Wallace, *Nat. Nanotechnol.*, 2008, **3**, 101-105.
32. X. Xiao, X. Peng, H. Jin, T. Li, C. Zhang, B. Gao, B. Hu, K. Huo and J. Zhou, *Adv. Mater.*, 2013, **25**, 5091-5097.
33. L. Qu, Y. Liu, J. B. Baek and L. Dai, *ACS Nano*, 2010, **4**, 1321-1326.
34. H. Wang, T. Maiyalagan and X. Wang, *ACS Catal.*, 2012, **2**, 781-794.
35. H. Liu, Y. Liu and D. Zhu, *J. Mater. Chem.*, 2011, **21**, 3335-3345.
36. Z. Lin, M. K. Song, Y. Ding, Y. Liu, M. Liu and C. P. Wong, *Phys. Chem. Chem. Phys.*, 2012, **14**, 3381-3387.
37. T. Okpalugo, P. Papakonstantinou, H. Murphy, J. McLaughlin and N. Brown, *Carbon*, 2005, **43**, 153-161.
38. T. Gao, F. Krumeich, R. Nesper, H. Fjellvåg and P. Norby, *Inorg. Chem.*, 2009, **48**, 6242-6250.
39. G. Zhou, D. W. Wang, L. C. Yin, N. Li, F. Li and H. M. Cheng, *ACS Nano*, 2012, **6**, 3214-3223.
40. W. Gao, N. Singh, L. Song, Z. Liu, A. L. M. Reddy, L. Ci, R. Vajtai, Q. Zhang, B. Wei and P. M. Ajayan, *Nat. Nanotechnol.*, 2011, **6**, 496-500.
41. D. Pech, M. Brunet, H. Durou, P. Huang, V. Mochalin, Y. Gogotsi, P. L. Taberna and P. Simon, *Nat. Nanotechnol.*, 2010, **5**, 651-654.
42. G. Wang, L. Zhang and J. Zhang, *Chem. Soc. Rev.*, 2012, **41**, 797-828.
43. X. Lu, M. Yu, T. Zhai, G. Wang, S. Xie, T. Liu, C. Liang, Y. Tong and Y. Li, *Nano Lett.*, 2013, **13**, 2628-2633.
44. M. Toupin, T. Brousse and D. Bélanger, *Chem. Mater.*, 2002, **14**, 3946-3952.
45. T. Brousse, P. L. Taberna, O. Crosnier, R. Dugas, P. Guillemet, Y. Scudeller, Y. Zhou, F. Favier, D. Bélanger and P. Simon, *J. Power Sources*, 2007, **173**, 633-641.
46. Y. Xu, Z. Lin, X. Huang, Y. Liu, Y. Huang and X. Duan, *ACS Nano*, 2013, **7**, 4042-4049.
47. L. F. Chen, Z. H. Huang, H. W. Liang, W. T. Yao, Z. Y. Yu and S. H. Yu, *Energy Environ. Sci.*, 2013, **6**, 3331-3338.
48. C. Meng, C. Liu, L. Chen, C. Hu and S. Fan, *Nano Lett.*, 2010, **10**, 4025-4031.
49. X. Xiao, T. Li, P. Yang, Y. Gao, H. Jin, W. Ni, W. Zhan, X. Zhang, Y. Cao and J. Zhong, *ACS Nano*, 2012, **6**, 9200-9206.
50. L. Yuan, X. H. Lu, X. Xiao, T. Zhai, J. Dai, F. Zhang, B. Hu, X. Wang, L. Gong and J. Chen, *ACS Nano*, 2011, **6**, 656-661.

A table of contents entry

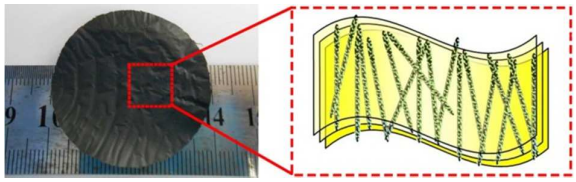

An all-solid-state SC based on flexible freestanding MNGHNs/AGO electrode with a volumetric capacitance as high as 26.3 F/cm^3 is developed.